To be published in Processing and Fabrication of Advanced Materials for High Temperature Applications, edited by T. S. Srivatsan and V. A. Ravi, The Minerals, Metals, and Materials Society, (2003).

# PROCESSING AND OXIDATION BEHAVIOR OF Nb-Si-B INTERMETALLICS

Yonghua Liu, Andrew J. Thom, Matthew J. Kramer, and Mufit Akinc

Ames Laboratory and
Department of Materials Science and Engineering
Iowa State University, Ames IA 50011

## Abstract

Single phase materials of $\alpha$-$Nb_5Si_3$ , $Nb_5(Si,B)_3$ (T2) and $Nb_5Si_3B_x$ ($D8_8$) in the Nb-Si-B system were prepared by powder metallurgy processing. T2 was almost fully dense, while $\alpha$-$Nb_5Si_3$ and $D8_8$ were porous after sintering at 1900°C for 2 hours. The lattice parameters of T2 decreased linearly with the substitution of B for Si. Isothermal oxidation testing at 1000°C in flowing air indicated that the oxidation resistances of T2 and $D8_8$ are much better than $\alpha$-$Nb_5Si_3$, but still extremely poor compared to the boron-modified $Mo_5Si_3$. Extensive cracking in the oxide scale and matrix were observed and arose from the volume expansion associated with the formation of $Nb_2O_5$ and boron-containing silica glass.

## Introduction

Transition metal silicides show good potential for use as structural materials at temperatures well in excess of 1000°C. Specifically, $M_5Si_3$ type compounds are attractive due to their high melting temperature and good creep resistance [1]. Disadvantages of single-phase $M_5Si_3$ compounds include brittle fracture at ambient temperature and poor oxidation resistance at elevated temperature. Some of these silicides can coexist with the refractory metal phase and therefore offer the potential for ductile phase toughening by forming M-$M_5Si_3$ composites. Two such candidates include Nb-$Nb_5Si_3$ and Ti-$Ti_5Si_3$. Since the Ti-Si system is not the topic of the present work, readers can refer to the work of Frommeyer et al. on the Ti-$Ti_5Si_3$ eutectic alloy [2]. The room temperature fracture toughness of Nb-$Nb_5Si_3$ composites range from about 8 $MPa{\cdot}m^{1/2}$ for a Nb-16Si alloy to about 21 $MPa{\cdot}m^{1/2}$ for a Nb-10Si alloy [3]. While the composites exhibit low temperature toughness, they still suffer poor oxidation resistance.

Research in our laboratory has shown that the addition of a small amount of boron to $Mo_5Si_3$ decreases the rate of oxidation by several orders of magnitude [4, 5]. The mechanism of improvement is the formation of a low-viscosity borosilicate glass that fills voids left by the evaporation of $MoO_3$ during the initial transient oxidation period. Boron additions of less than 2 wt% enable the formation of a continuous borosilicate scale that results in diffusion-limited oxidation kinetics. Boron additions to $Nb_5Si_3$ may have a similar effect.

The Nb-Si-B system was initially studied by Nowotny [6]. Two ternary phases form with large homogeneity regions, $Nb_5(Si,B)_3$ and $Nb_5Si_3B_x$, referred to as T2 and $D8_8$, respectively. Figure 1 shows the isothermal section of the Nb-Si-B phase diagram at 1600°C. The T2 phase has the $Cr_5B_3$-type tetragonal crystal structure in which boron substitutes for silicon, while the $D8_8$ phase has the $Mn_5Si_3$-type hexagonal crystal structure in which boron occupies an interstitial site. There exists a large region of equilibrium between the T2 phase and Nb metal.

Recently Murakami et al. [7] studied the oxidation behavior of compositions based on the $Nb_5Si_3$ ($D8_8$)-$NbB_2$-$NbSi_2$ phase triangle. Oxidation tests showed that the resistance increased in the sequence $NbB_2$, $Nb_5Si_3$, $D8_8$ and $NbSi_2$. The difference in oxidation behavior between boron-doped $Mo_5Si_3$ and boron-doped $Nb_5Si_3$ is related to the oxides formed. $Nb_2O_5$ remains as a condensed phase, in contrast to $MoO_3$, and rapidly grows to overwhelm the ability of the borosilicate glass to form a continuous and protective glass layer.

No definitive studies have investigated the oxidation behavior of the ternary T2 phase in the Nb-Si-B system. Therefore, the present study investigates the oxidation resistance of boron modified niobium silicides for long-duration

exposures in order to better evaluate the suitability of these materials in high temperature applications.

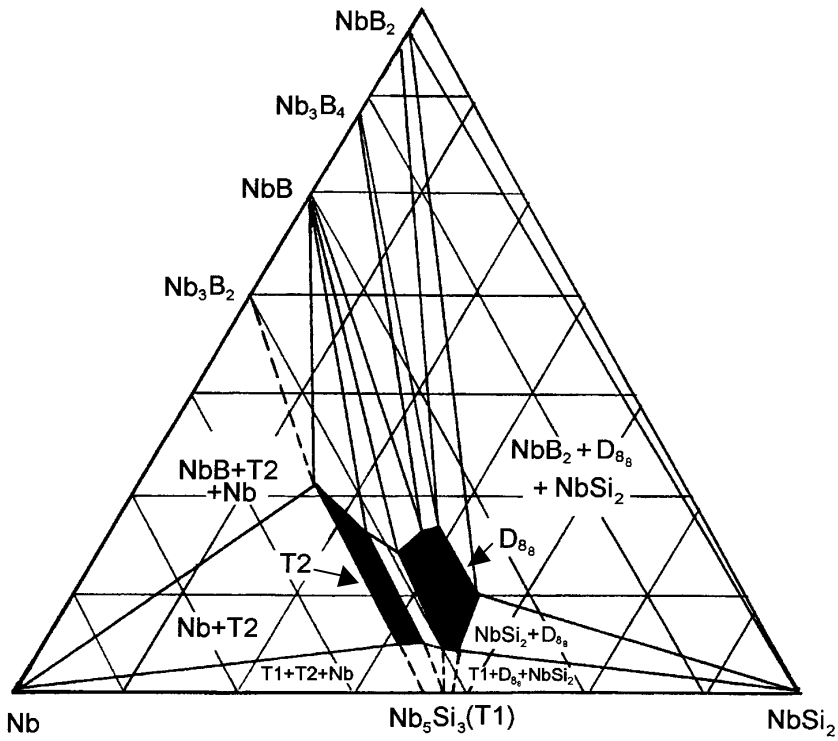


Figure 1. Isothermal section of Nb-Si-B system at 1600°C [6]

## Experimental Procedure

Six compositions in the Nb-Si-B system were chosen for study and these nominal compositions are shown in Table I. The starting materials used were 99.8% niobium rod, 99.99 % lump silicon and 99.5% lump boron. The samples were prepared from the starting materials by arc melting under argon on a copper hearth with a tungsten electrode. Before melting the elements, a zirconium button was melted to getter residual oxygen. Each sample was melted

at least three times to ensure homogeneity. The typical mass of an arc-melted button was about 25 g.

Table I: Nominal compositions (at.%) of Nb-Si-B samples

| Specimen | Expected phase assemblage | Nb | Si | B |
|---|---|---|---|---|
| 1 | $Nb_5Si_3$ | 62.5 | 37.5 | 0 |
| 2 | Nb + T2 | 70 | 20 | 10 |
| 3A | T2 | 63 | 27 | 10 |
| 3B | T2 | 62 | 23 | 15 |
| 4A | $D8_8$ | 56 | 32 | 12 |
| 4B | $D8_8$ | 55 | 30 | 15 |

Powder processing was performed inside an argon filled glove box with an oxygen content less than 1.0 ppm. The arc-melted buttons were milled in a tungsten carbide lined container with about 0.25 wt% stearic acid. Powders were sieved through a 635 mesh stainless steel sieve, with a nominal opening size of 20 µm, and uniaxially cold pressed into 0.95 cm diameter pellets at 186 MPa. Still inside the glove box, the samples were heated in a tube furnace to 550°C to remove the stearic acid under flowing high purity argon. Titanium sponge was placed near the pellets as a getter for nitrogen and oxygen. Pellets were then transferred to the sintering furnace without exposure to ambient air. Samples were sintered at 1900°C for 2 hours in a high temperature furnace under flowing high purity argon. The furnace was heated at 20°C/min and cooled at 5°C/min.

After sintering, porosity and bulk density of the pellets were measured using the Archimedes technique. Phase identification and microstructural characterization were performed using X-ray diffraction (XRD), scanning electron microscopy (SEM) and energy dispersive spectroscopy (EDS). Rietveld refinement of XRD pattern was performed using GSAS (General Structure Analysis System) to determine the fraction of phases present and the lattice parameters. Peak profile coefficients, thermal parameters, specific atom positions, and lattice parameters were varied to obtain the best numerical fit for the XRD data.

Oxidation samples were cut from the pellets and polished using standard metallographic techniques including a final polish with 0.05 µm $Al_2O_3$ abrasive.

A 0.18 mm diameter hole was drilled through coupons prior to polishing from which the coupons were suspended. The oxidation coupons, about 0.8 cm in diameter and 0.1cm thick, were suspended from a sapphire wire in a vertical tube thermogravimetric analyzer (TGA) that utilizes an electrobalance accurate to 1 x $10^{-5}$ g. Compressed breathing air was flowed over samples at 100ml/min. Specimens were heated at 20°C/min to 1000°C and held up to 120 hours. The oxidation-induced mass change was continuously recorded as a function of time. The chemical composition and microstructure of the oxide scale were characterized using XRD, SEM and EDS.

Table II: Density and phase analysis of sintered Nb-Si-B samples

| Sample | Major phase | Density, $g/cm^3$ | Relative density, % | Minor phase |
|---|---|---|---|---|
| 1 | $\alpha$-$Nb_5Si_3$ | 5.5 | 78 | Hex-$Nb_5Si_3$: 2 vol% |
| 2 | T2 | 7.4 | 98 | Nb, 20 vol.% |
| 3A | T2 | 6.9 | 95 | Nb, 3 vol.% |
| 3B | T2 | 7.0 | 96 | Nb, 2 vol.% |
| 4A | $D8_8$ | 5.4 | 77 | NbB, 3 vol.% |
| 4B | $D8_8$ | 5.4 | 77 | NbB, 8 vol.% |
| 4B* | $D8_8$ | 6.0 | 84 | NbB, 19 vol.% |
| 4B** | $D8_8$ | 6.1 | 85 | NbB, 3 vol.%, + |

4B*: sintered at 2100°C for 1 hour
4B**: hot pressed at 1700°C for 1 hour under 100 MPa
+: has a large amount of unidentified phase ( > 10% approximately)

## Results and Discussion

### Phase analysis and microstructure

The results of Archimedes density measurements and phase analysis with XRD are presented in Table II. The minor phase component is listed for each sample, and the relative density was calculated using the theoretical density derived from the GSAS refinement. Sample 1 contains mainly low temperature $\alpha$-$Nb_5Si_3$ ($D8_l$ $Cr_5Si_3$-type structure).

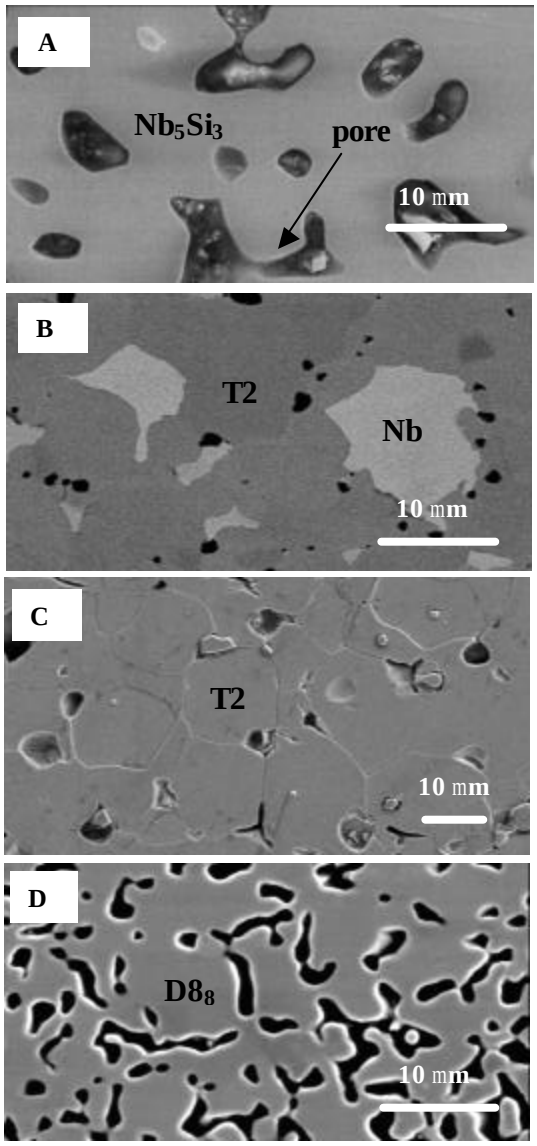


Figure 2. SEM micrographs of Nb-Si-B specimens sintered at 1900°C for 2 hours. (a) Sample 1; (b) Sample 2; (c) 3A; (4) 4A. The dark areas are pores.

The presence of about 2 vol.% of hexagonal $Nb_5Si_3$ is most likely the result of residual carbon from incomplete removal of the stearic acid. Carbon is known to stabilize the $Mn_5Si_3$-type hexagonal structure in $Mo_5Si_3C_x$ [8, 9]. A similar stabilization effect in $Nb_5Si_3$ is also expected. Unlike $Mo_5Si_3$, which can be sintered to near theoretical density at 1800°C [5], the density of $Nb_5Si_3$ was much lower at 78% of theoretical density in this study, even though material was sintered at 1900°C for 2 hours. Figure 2a shows single-phase $\alpha$-$Nb_5Si_3$ with a significant amount of porosity. To a first order, the difference in sintering behavior between $Nb_5Si_3$ and $Mo_5Si_3$ can be attributed to the difference in their melting temperatures. $Mo_5Si_3$ has a melting point of 2180°C, whereas the melting point of $Nb_5Si_3$ is 2515°C. The higher melting temperature of $Nb_5Si_3$ predicts slower diffusion at a given temperature in $Nb_5Si_3$ compared to $Mo_5Si_3$. Fitzer [10] reported that the coefficient of silicon diffusion in $M_5Si_3$ transition metal silicides decreased on the order: $Mo_5Si_3 > W_5Si_3 > Nb_5Si_3 > Ta_5Si_3$. Metal interdiffusion in these $M_5Si_3$ materials was much slower compared to silicon diffusion.

Sample 3A and 3B are nearly single phase T2 with about 1 to 3 vol. % metal phase Nb. The grain size of T2 is 20-30 μm, seen in Figure 2c, and sample 2 contains about 20 vol. % pure Nb in a T2 matrix, seen in Figure 2b. No cracks were observed in these samples, and this suggests that T2 has a lower extent of thermal expansion anisotropy. Zhao reported [11] that the thermal expansion anisotropy $\alpha_c/\alpha_a$ is about 0.93 for T2 in Mo-Si-B system. Similar thermal expansion behavior is expected for T2 in Nb-Si-B system. Samples 2, 3A and 3B have bulk density values greater than 95% of theoretical density. This suggests that diffusion in the boron-containing T2 phase is faster than in boron-free $Nb_5Si_3$, but there is no diffusion data available for the T2 phase to quantify this assertion.

Samples 4A and 4B are nearly single phase $D8_8$ with 3-8 vol. % NbB as the minor phase. The sintered samples are porous and their density is similar to that of $\alpha$-$Nb_5Si_3$. A higher sintering temperature of 2100°C and hot pressing at 1700°C under 100 MPa were employed to increase density. However, the density increased only slightly to about 85% of theoretical. Hot pressed sample 4B contained an appreciable amount of an unidentified phase. Because the sample was hot pressed in a graphite die, formation of a carbide phase is suspected. Because the complete phase assemblage could not be refined, the reported density value can only be considered as a rough indication.

Murakami and Yamaguchi [7] reported that the density of composition Nb-34Si-10B ($D8_8$), which is close to sample 3A in this study, was greater than 90% of theoretical by using spark plasma sintering between 1500° and 1800°C.

However, in their study a large amount of $SiO_2$ was observed in the microstructure, and this may behave as a sintering aid. The application of 49 MPa pressure at 1700°C likely contributed to viscoplastic deformation of silica in the compacts and thus greatly increased density. Like monolithic $\alpha$-$Nb_5Si_3$, the lower sintered density of $D8_8$ suggests slower diffusion and a high melting point, although no data has been reported for the $D8_8$ phase. For specimens containing $D8_8$ as the matrix phase, the fraction of NbB increases as processing temperature increases from 1700°C to 2100°C. This suggests that the boron content of the homogeneity region of $D8_8$ decreases as temperature increases.

**Lattice constants**

The composition of the T2 and $D8_8$ phase in each sample was calculated by subtracting the minor phase compositions from the overall composition obtained by the XRD/GSAS analysis. Table III shows these corrected compositions and the lattice parameters for niobium silicides for the T2 and $D8_8$ phases.

Table III: Phase compositions and lattice parameters for T2 and $D8_8$

| Sample | Phase | Compositions, at% | | | | Lattice parameters, Å | |
|---|---|---|---|---|---|---|---|
| | | Nb | Si | B | B/Si | a | c |
| Ref 8 | T2 | | | | | 6.570 | 11.887 |
| 1 | T2* | 62.5 | 37.5 | 0 | 0 | 6.571(6) | 11.887(7) |
| 2 | T2 | 62.9 | 24.7 | 12.3 | 0.50 | 6.435(2) | 11.778(4) |
| 3A | T2 | 62.0 | 27.6 | 10.2 | 0.37 | 6.468(7) | 11.806(5) |
| 3B | T2 | 61.5 | 23.2 | 15.1 | 0.65 | 6.404(0) | 11.753(5) |
| 4A | $D8_8$ | 56.2 | 33.2 | 10.5 | 0.32 | 7.590(7) | 5.271(2) |
| 4B | $D8_8$ | 55.5 | 33.3 | 11.1 | 0.33 | 7.593(9) | 5.273(3) |
| 4B* | $D8_8$ | 56.5 | 38.6 | 4.9 | 0.13 | 7.566(7) | 5.264(3) |

T2*: boron free $\alpha$-$Nb_5Si_3$
4B*: sintered at 2100°C for 1 hour

The lattice parameters of $\alpha$-$Nb_5Si_3$ are in good agreement with the literature [12]. The co-existence of T2 with Nb metal in samples 2, 3A and 3B suggests that the lattice parameters of T2 refer to the Nb-rich boundary of the T2 phase field. Figure 1 shows that at 1600°C the Nb-rich boundary of the T2 phase varies over a large B/Si range but over a much smaller Nb content. The calculated compositions of T2 in Table III confirmed this result, and thus the

difference in lattice parameters for T2 in this study are most likely related to changes in boron and/or silicon contents. Figure 3 shows that the unit cell volume of the T2 phase decreases linearly with the increase of B/Si ratio, suggesting that boron atoms substitute onto silicon lattice sites. Similarly, the co-existence of NbB and $D8_8$ suggests that the lattice parameters of $D8_8$ in this study correspond to the B-rich boundary of the $D8_8$ phase field. Since the boron composition of samples 4A and 4B changes by only 0.6 at%, only small changes in lattice parameters for $D8_8$ are expected. In the hexagonal $D8_8$ structure of $Ti_5Si_3B_x$, boron occupies an interstitial site and significantly expands the lattice [13]. Sample 4B has a slightly higher calculated boron content than Sample 4A, and this is consistent with the increased cell volume of sample 4B. As discussed previously, the phase field of $D8_8$ moves toward lower boron content with the increase in temperature, and thus the lattice parameters of $D8_8$ in sample 4B* are much smaller than those in 4A and 4B. From this study, the boron solubility in $D8_8$ decreases from about 11 at. % at 1900°C to about 5 at. % at 2100°C.

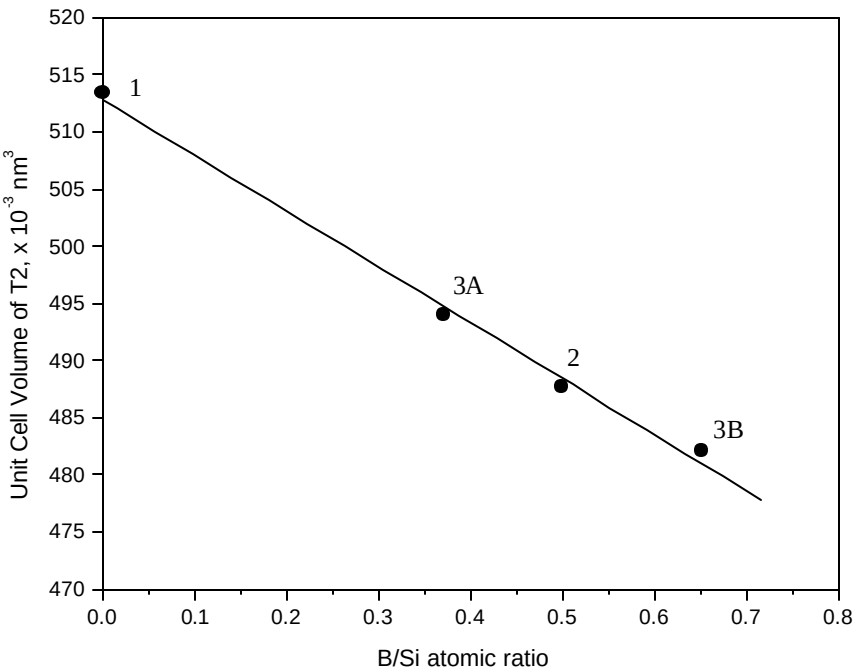


Figure 3. Unit cell volume change as a function of B/Si atomic ratio for T2 phase in samples 1, 2, 3A and 3B.

**Oxidation**

Figure 4 shows the oxidation-induced mass gain for five studied compositions in Nb-Si-B system at 1000°C in flowing air as a function of time. The mass curves were fitted to either a parabolic model or a linear model, and the fit of the model is indicated by the correlation coefficient R in Table IV. Sample 1 underwent a rapid mass gain of 17.7 $mg/cm^2/h$. The outer layer disintegrated to powder, and after about 3 hours the sample fell out of the furnace, and so no further data was collected for this sample. A similar result was also reported by Jackson [14] for which arc melted $Nb_5Si_3$ crumbled after one hour exposure in air at 1000°C. Sample 4A showed better oxidation resistance than $Nb_5Si_3$, although it had a sintered density similar to $Nb_5Si_3$. Sample 4A exhibited parabolic kinetics, but its large rate constant of 15 $mg^2/cm^4/h$ indicated that the scale formed was not protective. Sample 3A had a much higher sintered density than sample 4A, but it exhibited only a slightly lower mass gain. Sample 3B had a higher B/Si ratio than sample 3A, and the linear rate increased by nearly a factor of three. The higher B/Si ratio of 3B implied a higher fraction of $B_2O_3$ in silica glass. The lower anticipated scale viscosity was insufficient to protect the sample. Sample 2 (T2 + 20 vol. %Nb) oxidized much more rapidly than the T2 and $D8_8$ containing samples. After 50 hours, the specimen was almost completely consumed, presumably due to the substantial Nb metal phase content.

X-ray diffraction detected only $Nb_2O_5$ in the yellow-white surface oxide scales of all samples, and no crystalline silica was detected by XRD. SEM and EDS analysis of the cross sections of oxidized specimens showed that the scale is composed of a very fine mixture of $Nb_2O_5$ and borosilicate glass. The scale thickness is about 400 μm for sample 3A after 125 hours oxidation at 1000°C. The differences in standard free energy of formation between $Nb_2O_5$, $SiO_2$ and $B_2O_3$ are not significant [15], and Nb, Si and B likely oxidize simultaneously to form the fine mixture of $Nb_2O_5$ and borosilicate glass.

Scale spalling was not observed in the boron-containing specimens after cooling from the oxidation temperature. However, severe cracks were observed in both the scale and matrix of sample 3A. This cracking in the T2 phase is a consequence of the volume expansion associated with the formation of $Nb_2O_5$, $SiO_2$ and $B_2O_3$. Based on reaction Eq. 1,

$$2\ Nb_5Si_3B + 20\ O_2 = 5\ Nb_2O_5 + 6\ SiO_2 + B_2O_3 \qquad (1)$$

the volume of oxide products is almost 3 times greater than the volume of the matrix material. Oxide growth would lead to a tensile stress in the silicide matrix

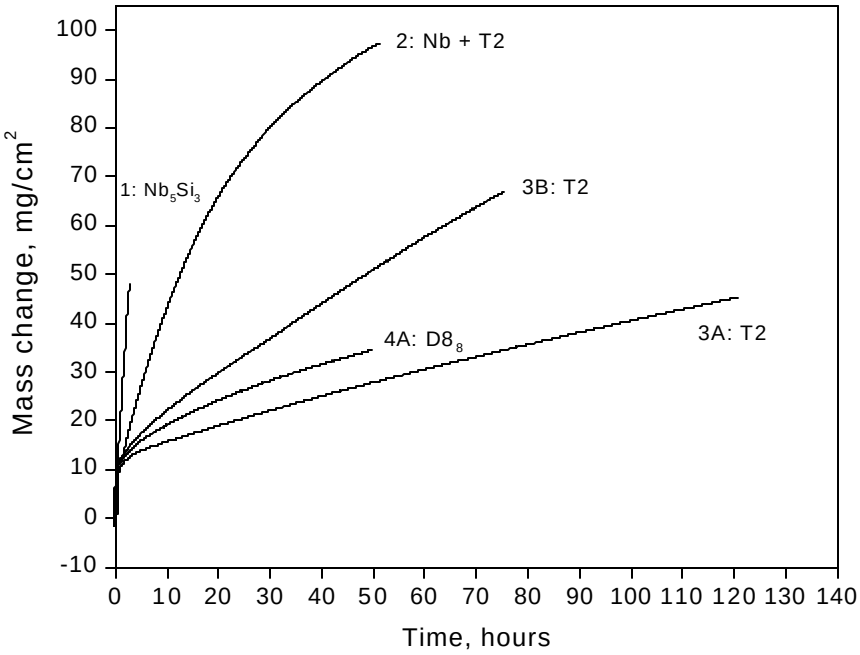


Figure 4. Oxidation-induced mass change of Nb-Si-B samples at 1000°C in flowing air.

and a compressive stress in the scale along scale/matrix interface. The ensuing matrix cracking accelerated the rate of oxidation and contributed to the linear mass gain. The extensive cracking in the scale was most likely due to the thermal stresses during cooling. The thermal expansion coefficient of $Nb_2O_5$ is four times smaller than that of $Nb_5Si_3$ [16], and the scale formed on T2 will likely spall in a cyclic oxidation test.

Because sample 3A is much denser than sample 4A, sample 4A is expected to have a larger initial mass gain. However, no significant difference in mass gain was measured. One plausible explanation is that sample 4A has a larger (Si + B)/Nb ratio than sample 3A, and thus more borosilicate glass is expected in the scale. The borosilicate glass would seal some of the cracks in the matrix, and

subsequently decrease the oxygen transport through the scale. The coefficient of oxygen diffusion in $Nb_2O_5$ (8.7 x $10^{-11}$ $cm^2$/sec) is almost 1000 times higher than in silica glass (1.8 x $10^{-14}$ $cm^2$/sec) at 1000 °C [17, 18]. The oxidation process is most likely dominated by the diffusion of oxygen through $Nb_2O_5$. In this study, the fact that T2 and $D8_8$ have much better oxidation resistance than binary α-$Nb_5Si_3$ suggests that additions of boron can improve the oxidation resistance of niobium silicides, although the improvement is limited. The difference in oxidation resistance between boron-doped $Mo_5Si_3$ and boron-modified niobium silicide is most likely due to the $Nb_2O_5$, which has a melting point 1460°C and does not volatilize. The rapid formation and growth of $Nb_2O_5$ competes with the temperature-induced reflow of the lower viscosity borosilicate glass. As a result, a continuous protective borosilicate layer does not form on the surface of material, and therefore rapid oxygen transport occurs through the scale.

Table IV: Rate constants of the Nb-Si-B specimens oxidized at 1000°C

| Sample | Major Phase | Time Period | Parabolic | | Linear | |
|---|---|---|---|---|---|---|
| | | | $K_p$ | $R^2$ | $K_l$ | $R^2$ |
| 1 | $Nb_5Si_3$ | 1-3 | | | 17.7 | 0.991 |
| 2 | Nb + T2 | 2-50 | 215 | 0.987 | | |
| 3A | T2 | 3-125 | | | 0.25 | 0.995 |
| 3B | T2 | 2-75 | | | 0.71 | 0.997 |
| 4A | $D8_8$ | 1-50 | 15 | 0.999 | | |

$K_p$: parabolic rate constant, $mg^2/cm^4/h$
$K_l$: linear rate constant, $mg/cm^2/h$

## Summary

Powder compacts of α-$Nb_5Si_3$ , T2-$Nb_5(Si,B)_3$ and $D8_8$-$Nb_5Si_3B_x$ were prepared by sintering arc-melted and reground material at 1900°C for 2 hours. The T2 phase was almost fully dense, while α-$Nb_5Si_3$ and $D8_8$ were porous, and this reflects slower diffusion in α-$Nb_5Si_3$ and $D8_8$ compared to T2. A Nb-reinforced T2 composite was also produced, but no fracture toughness tests were made to quantify any ductile-phase toughening of the brittle T2 silicide. For a

constant Nb content, the lattice volume of T2 decreased linearly with an increase in the B content. The boron-free $\alpha$-$Nb_5Si_3$ displayed pest oxidation at 1000°C in air. Boron-containing phases, T2 and $D8_8$, showed better oxidation resistance than $\alpha$-$Nb_5Si_3$, but they are still extremely poor compared to boron-modified $Mo_5Si_3$. The oxide scale was composed of a fine mixture of $Nb_2O_5$ and borosilicate glass. Extensive cracking in the oxide scale and matrix for the T2 composition is most likely related to the volume expansion associated with the formation of the oxides.

## Acknowledgements

This manuscript has been authored by Iowa State University of Science and Technology under contract No. W-7405-ENG-82 with the U.S. Department of Energy. The United States Government retains and the publisher, by accepting the article for publication, acknowledges that the United States Government retains a non-exclusive, paid-up, irrevocable, worldwide license to publish or reproduce the published form of this manuscript, or allow others to do so, for United States Government purposes.

## References

1. D. M. Shah, Superalloys. ed. S. D. Antolovich et al. The Mineral, Metals and Materials Society, Warrendate, PA, 409, 1992.

2 G. Frommeyer, R. Rosenkranz, C. Ludecke, "Microstructure and Properties of the Refractory Intermetallic $Ti_5Si_3$ Compound and the Unidirectionally Solidified Eutectic Ti-$Ti_5Si_3$ Alloy," Z. Metallkde. 81, 307-313, 1990.

3. M.G. Mendiratta, J.J. Lewandowski and D.M. Dimiduk, " Strength and Ductile-Phase Toughening in the Two-Phase Nb/$Nb_5Si_3$ Alloys ", Metall. Trans, 22A, 1573-1583, 1991.

4. M.K. Meyer, A.J. Thom and M.Akinc, "Oxidation Scale formation and isothermal Oxidation behavior of Mo-Si-B Intermetallics at 600-1000°C", Intermetallics, 7, 153-162, 1999.

5. M.K. Meyer and M.Akinc, "Oxidation behavior of boron-modified $Mo_5Si_3$ at 800-1300°C", J. Am. Ceram. Soc., 79[4], 938-944, 1996.

6. H.Nowotny, F. Benesovsky, E. Rudy and A. Wittmann, "Aufban und Zunderverhalten von Noib-Bor-Silicium Legierungen", Monatch. Chem., 91, 975-990, 1960.

7. T. Murakami, C. N. Xu, A. Kitahara, M. Kawahara, Y. Takahashi, H. Inui, M. Yamaguchi, "Microstructure, Mechanical Properties and Oxidation Behavior

of Power Compacts of the Nb-Si-B System Prepared by Spark Plasma Sintering", Intermetallics, 7, 1043-1048, 1999.
8. H. Nowotny, E. Parthé, R. Kieffer, and F. Benesovsky, Mh. Chem. 85, 255-272, 1954.
9. E. Parthe, W. Jeitschko, V. Sadagopan, "A Neutron Diffraction Study of the Nowotny Phase Mo<5Si3C<1," Acta Cryst. 19, 1031-1037, 1965.
10. E. Fitzer and F.K.Schmidt, "Die Siliziumdiffusion in den $Me_5Si_3$ –Phasen der Metalle Niob, Tantal, Molybdan und Wolfram bis 1700 °C", High Temperature-High Pressures, 3, 445-460, 1971.
11. H.L. Zhao, Thermal Expansion Behavior of Mo-Si-B Intermetallics, M.S Thesis, Iowa State university, Ames, IA, 2001.
12. Card 30-0874, JCPDS-International Center for Diffraction Data, Newtowne Square, PA, 1993.
13. A.J. Thom, V.G. Young, and M. Akinc, "Lattice Trends in $Ti_5Si_3Z_x$ (Z=B,C,N,O and 0<x<1)," Journal of Alloys and Compounds 296, 59-66, 2000.
14. M. R. Jackson, R.G. Rowe, and D.W. Skelly, " Oxidation of Some Intermetallic Compounds and Intermetallic Matrix Composites", Mat. Res. Soc. Symp. Proc., 364, 1339-1344, 1995.
15. I. Barin, Thermochemical Data of Pure Substances, 2nd ed. Weinhiem; New York: VCH (1993).
16. D.L. Douglass, "The Thermal Expansion of Niobium Pentoxide and Its Effect on the Spalling of Niobium Oxidation Films", J. Less-Common Metals, 5, 151-157, 1963.
17. F.H.Wohlbier, Diffusion and Defect Data, 14, 129, 1977.
18. F.H.Wohlbier, Diffusion and Defect Data, 17, 135, 1978.